

Special Issue on New Challenges in Energy Materials

# Key issues to high electroactivity for methanol oxidation and oxygen reduction of Pt-based supported catalyst in fuel cells relevant environment

A.I. de Sá<sup>a</sup>, A. Capelo<sup>a</sup>, A. Esteves<sup>a</sup>, L. Cangueiro<sup>b</sup>, A. Almeida<sup>b</sup>, R. Vilar<sup>a</sup>, C.M. Rangel<sup>\*</sup>

<sup>a</sup>Laboratório Nacional de Energia e Geologia (LNEG), Paço do Lumiar, 22, 1649-038 Lisboa, Portugal

<sup>b</sup>Instituto Superior Técnico (IST), Av. Rovisco Pais, 1049-001 Lisboa, Portugal

## Abstract

In this work some of the key issues which affect the performance of catalysts for the anode and cathode electrodes in Direct Methanol Fuel Cells are analyzed. To deal with present challenges and overcome limitations different approaches have been implemented, which include catalyst support diversification and functionalization, control of particle size and the introduction of Pt alloying and heat treatment in order to enhance the rate of critical reactions such as CO electrooxidation and oxygen reduction reaction and also reduce Pt loading. A catalyst design strategy has been devised which incorporates the mentioned approaches in order to tackle various critical aspects for both electroactivity and stability, considered essential to boost Direct Methanol Fuel Cells technology.

© 2016 Portuguese Society of Materials (SPM). Published by Elsevier España, S.L.U.. All rights reserved.

*Keywords:* Methanol oxidation; Pt-based catalyst; carbon functionalization; oxygen reduction.

## 1. Introduction

Direct Methanol Fuel Cells (DMFCs) are electrochemical devices where methanol oxidation occurs to produce electricity and heat. Basically, the device is similar to a battery since it converts the chemical energy of fuel and oxidant into electric energy; yet unlike batteries, fuel cells do not need recharging: the fuel is continuously supplied to the anode and the oxidant to the cathode. Methanol oxidation occurs with the release of protons and electrons; the protons go through a conductive membrane to the cathode, where oxygen is introduced and reduced to form water; the electrons go through the external circuit and correspond to energy produced that can be converted into work. The main disadvantage is the release of CO<sub>2</sub> as the product of the methanol oxidation reaction (MOR). However, in a

sustainable energy future, the cells should be associated with carbon capture and recycling (CCR) technology, closing the loop of harmful emissions [1,2] with methanol being produced from renewable sources [3].

DMFCs have some advantages when compared to hydrogen fuel cells: methanol can be transported and store in liquid phase, using the infrastructure for liquid fuels already available [4,5]. This flexibility on fuel handling makes this technology not only attractive for large scale energy production and transportation, but well suited for small portable applications, for example in consumer electronic devices [4-8]. The DMFCs are projected to reach a market of USD 188.82 Million by 2020 [9]. The portable application market segment is expected to show the highest growth rate with DMFCs, called to fill in the gap between energy demand and energy storage capacity. The energy density of methanol is higher than that of hydrogen [8] and also of lithium ion batteries [6,7]. Apart from that, easy/short time refueling and cold

\* Corresponding author.

E-mail address: [carmen.rangel@lneg.pt](mailto:carmen.rangel@lneg.pt) (C.M. Rangel)

start are considered substantial advantages driving DEMFCs technology development.

For the continuous market increase of DMFCs for portable applications, challenges include reducing noble metal catalyst loading for lower cost, reducing methanol crossover for increased efficiency, simplifying the BOP for increased energy and power density and improved reliability [8]. So far, the best catalysts are still based on supported Pt nanoparticles, which are prone to CO poisoning on the anode side [10–13]. On the cathodic side, the sluggishness of the oxygen reduction reaction (ORR) kinetics also demands catalysts with a more efficient chemical-to-electrical energy conversion to contribute to necessary improvements in cell performance and lifetime [14,15].

In this work some of the key issues which affect the performance of catalysts for the anode and cathode electrodes in DMFCs are analyzed. To deal with the mentioned challenges and overcome limitations different approaches have been implemented, which include catalyst support diversification and functionalization, control of particle size and the introduction of Pt alloying in order to enhance the rate of critical reactions in DMFCs such as CO electrooxidation (COR) and ORR and also to reduce Pt loading. A catalyst design strategy has been devised which incorporates the mentioned approaches in order to tackle various critical aspects for both electroactivity and stability, considered essential to boost DMFC technology.

## 2. Catalyst design

### 2.1. Introduction

Although the thermodynamic potential for the electro-oxidation of methanol in acid electrolytes is close to that of hydrogen oxidation, the overall reaction is very demanding due to the multi-electron transfer to form carbon dioxide. The half reaction is:



The generally accepted mechanism for the methanol oxidation reaction (MOR) on Pt catalysts proceeds with the electroadsorption of methanol, followed by proton and electron stripping. Dehydrogenation and insertion of oxygen into the adsorbed methanol fragment, as well as removing six electrons from each molecule are necessary for full oxidation. The transfer of electrons occurs in a step-wise manner, giving rise to the formation of surface adsorbed species which act as poisons for ensuing methanol adsorption and oxidation. Water is co-adsorbed

at neighboring sites to the bound CO and oxygen transfer occurs to give CO<sub>2</sub>, which desorbs from the catalyst surface. At potentials below ca. 0.45 V vs. RHE, the surface of Pt becomes poisoned with a near-monolayer coverage of CO and further adsorption of water or methanol cannot occur. Rapid decay of the current, as a result of the formation of strongly bound intermediates, is found for clean Pt surfaces which, initially, show very high activity for the MOR [4,5].

The development of advanced Pt-based catalysts has been focused, for some time, on the addition of a second metal (Ru, Sn, W, Re) able to provide adsorption sites capable of forming OH<sub>ads</sub> species, at low potentials, adjacent to poisoned Pt sites. The OH<sub>ads</sub> is then able to react with the bound CO to produce CO<sub>2</sub> and free sites for further methanol adsorption. For promoters such as Ru, stable methanol oxidation currents occur at significantly lower potentials (<0.25 V vs. RHE) than Pt. In this work enhancement of the catalytic activity of own produced Pt-Ru catalyst will be discussed in section 5. Regarding the ORR, mechanism pathways are briefly introduced, in section 6, for Pt and alternative Pt-based alloys with high selectivity, which may safeguard generation of water as the only by-product, stability and durability so that maximum power output in fuel cells is ensured.

More recent efforts have been focused on how to use platinum more effectively. In general, to achieve the maximum number of active sites of a given active phase, dispersion of that phase on an inert support is required. In the case of low-temperature fuel cells, the support is required to provide high surface area, high level of catalyst dispersion, facilitate electron transport during electrochemical reactions, porous structure for maximum fuel contact and product release. Also good electronic conductivity and corrosion resistance are paramount to maintain a good catalyst-support interaction and high stability in fuel cell environment [4,5]. These requirements are generally met by conductive carbon supports, which allow the active phase to be dispersed finely over the support surface. In this work, in the context of the mentioned requirements, Vulcan XC-72 and multi-walled carbon nanotubes (MWCNTs) are the catalyst supports of choice.

### 2.2. Support functionalization

As already stated, to achieve high efficiency and stability in DMFCs, catalysts, for both MOR and ORR, are prepared in the nanosized range and dispersed on high surface area carbon supports [4,5,16].

Carbon based supports such as Vulcan XC-72, mesoporous carbons, carbon nanofibers, carbon nanotubes, carbon nanosphere and more recently graphene, have attracted much attention in the last decades since they exhibit good physical properties as well as abundance, environmental friendliness and good stability [17-20]. Recent results [21-23] have shown that the chemical modification of the surface of carbon supports promotes a good distribution of the catalyst and consequently an improvement in performance. A wide variety of functionalized nanocarbons have been reported in the literature in recent years, mainly obtained by covalent and non-covalent functionalization or by heteroatom surface doping methods [23-25]. Surface functionalization, namely, by the addition of organic functionalities is an efficient way to make these materials more versatile by optimizing the bulk and interfacial properties and promoting the interactions with guest molecules [21, 23]. Generally, covalent functionalization is preferable because it yields composites with better stability and structure control. In particular, surface carboxyl groups can be used to couple amino organic, via conversion of the carboxyl group of the surface to an acyl chloride, which subsequently react with the primary amino group of the organic compound to form an amide covalent bond [21]. This method can be used for a wide range of carbon materials allowing improvements in electronic conductivity when compared with supports subjected to chemical oxidation only. This type of reaction is for instance an efficient way to introduce N-heterocycles and heteroatoms (N, O, S) on the carbon support surface.

The electrocatalysts presented in this work were designed following two main approaches: new functionalized supports to promote effective dispersion (Pt and alloys) and Pt load reduction by using alloying applied to both the MOR (Pt-Ru) and ORR (Pt-Ni).

Vulcan XC-72 and multi-walled carbon nanotubes were functionalized with ionic liquid 1-(3-aminopropyl)-3-methyl-imidazolium bromide, here designated by C\_IL and MWCNT\_IL. Vulcan XC-72 was also functionalized using less studied aromatic nitrogen and sulphonic groups and is referred to as C\_ABSA. The functionalization methods were optimized using Vulcan XC-72 as starting material, and then applied to MWCNTs. Briefly, in the first step, the oxidation of the carbon materials with HNO<sub>3</sub> is implemented in order to introduce carboxylic acid groups in the surface. In the next step, the previously prepared IL [26], is covalently attached to the oxidized carbon, C-COOH [27] through an amidation reaction

between the carboxylic acid surface group and the IL amino group. The IL loading in the functionalized carbons, calculated from the amount of nitrogen in the solid found by elemental analysis, varied between 0.4 and 0.5 mmol g<sup>-1</sup>.

C\_ABSA has been prepared from C\_COCl, see scheme 1, to this end it was added an excess of 4-aminobenzenesulphonic acid to the dried C\_COCl, this mixture was refluxed in toluene [21]. An ABSA loading on the functionalized carbon C\_ABSA, 1.06 mol g<sup>-1</sup>, was estimated from the amount of nitrogen and sulphur in the solid by elemental analysis.

Experimental procedure used for the functionalization of the carbon materials, Vulcan XC-72 and MWCNTs, is summarized in Figure 1, together with the catalyst synthesis. The latter is described more in detailed in the following section.

### 2.3. Catalyst synthesis

From the many methods applied to the preparation of carbon supported fuel cell catalysts, the present discussion is restricted to the preparation of Pt-based catalysts by chemical synthesis methods, due to their relatively easy and inexpensive implementation. Table 1 includes some of the most common chemical methods found in the literature namely the impregnation, colloidal and microemulsion methods.

The catalytic activity is controlled by the surface composition as well as the size and dispersion of the nanoparticles which are highly dependent on the used catalyst synthesis methods and reducing agents [28,29,30-42]. Some examples are given below.

For catalysts supported on carbon nanofibers (Pt-Ru/CNF), the influence of the reduction method in the characteristics of the catalysts using the impregnation method have been studied [28]. Three different reduction agents were used: sodium borohydride (BH), formate ion (SFM) and methanol (MeOH). The results showed that nanoparticles sizes of ca. 4 nm were obtained by the BH and SFM methods while for the MeOH method the particles tend to be smaller (ca 3 nm). Heat treatment of the samples increased particle size up to ~ 7 nm. In the synthesis of Pt using mesoporous carbon xerogels as support, the use of the impregnation method, using formic acid as reducing agent [29], revealed that catalysts show good metallic distribution and particle sizes of ca. 3.6 nm, smaller than in the case of the microemulsion method [29] with a size of ca. 3.9 nm. The latter showed a higher electroactivity for COR and MOR. The colloidal method also reported in Table 1, is particularly

adequate for the synthesis of small size metal nanoparticles (2-3 nm) [43,44]. The impregnation method usually produces NPs with large average particle sizes and broad size distributions while the colloidal route produces well-homogenized ultrafine Pt electrocatalysts, however, the complexity of the latter method hinders its utilization.

Table 1. Most frequently used chemical methods for catalyst synthesis.

Synthesis method	Brief description	Ref.
Impregnation one of the simplest and most widely used methods (broad size particle distribution)	Solution of metal salt(s) precursors mixed with carbon support followed by solvent removal. Heat-treatment and/or reduction of the salt are promoted to give desired catalyst. Suitable reducing agents are $\text{NaBH}_4$ , ethyleneglycol, formic acid, etc.	[28-42]
Colloidal extensively used method (well-homogenized, ultra-fine particles)	Preparation of Pt–metal colloids, followed by deposition of the colloids onto the carbon support and chemical reduction of the suspension.	[43,44]
Microemulsion “water in oil” particle size can be controlled by the micro-emulsion magnitude	Formation of Pt–based NPs through a water-in-oil microemulsion reaction by a reduction step ( $\text{N}_2\text{H}_4$ , HCHO or $\text{NaBH}_4$ ) confined in the microemulsion system. The removal of surfactant molecules can be done by heat treatment.	[29]

As already stated, a Pt and two bi-metallic (Pt-Ru, Pt-Ni) catalysts were synthesized by metal deposition on two different organic functionalized carbon materials, prepared as indicated in section 2.2, using different reduction agents. Some details of the preparation are given below.

A Pt-Ru supported catalyst with a nominal composition of 10 wt.% Ru and 20 wt.% Pt was prepared using the ethyleneglycol (EG) reduction method in a three step procedure. In the first step, nanoparticles of Ru were synthesized by reduction of  $\text{RuCl}_3$  with EG at 160 °C for 5 h and pH 11. Then, Ru-Pt nanoparticles were obtained by deposition of Pt in the surface of the Ru nanoparticles using  $\text{PtH}_2\text{Cl}_6 \cdot 6\text{H}_2\text{O}$  as the precursor salt and EG as reduction agent. In the final step, the Ru-Pt nanoparticles were deposited in the functionalized

carbon support by a simple adsorption process at acidic conditions [38].

For the synthesis of Pt-Ni nanocatalysts with a nominal Ni/Pt atomic ratio of 10:3, it was used a modified polyol/potassium borohydride reduction method previously described [12]. In the first step Ni nanoparticles supported in the IL functionalized carbons ( $\text{C}_{\text{IL}}$ ) were prepared in propyleneglycol at 138 °C at basic pH, using potassium borohydride as reducing agent and oleic acid as capping agent. The second step consisted in the platinum deposition on the Ni/ $\text{C}_{\text{IL}}$  particles, at mild reduction conditions using  $\text{H}_2\text{PtCl}_6 \cdot 6\text{H}_2\text{O}$  in propyleneglycol at 138 °C.

The Pt/ $\text{C}_{\text{ABSA}}$  catalyst, with a nominal composition of 20 wt.%, was prepared with  $\text{H}_2\text{PtCl}_6 \cdot 6\text{H}_2\text{O}$  as a platinum precursor, using formic acid as reduction agent. In this method ABSA functionalized carbons ( $\text{C}_{\text{ABSA}}$ ) was dispersed in formic acid and subsequently platinum (with  $\text{H}_2\text{PtCl}_6 \cdot 6\text{H}_2\text{O}$ ) was deposited on the surface of  $\text{C}_{\text{ABSA}}$  at 80 °C [21].

The whole process used for support functionalization and catalyst synthesis is summarized in Figure 1. Commercial catalysts supported on Vulcan with 10 and 20 wt.% Pt loading were also used for comparison.

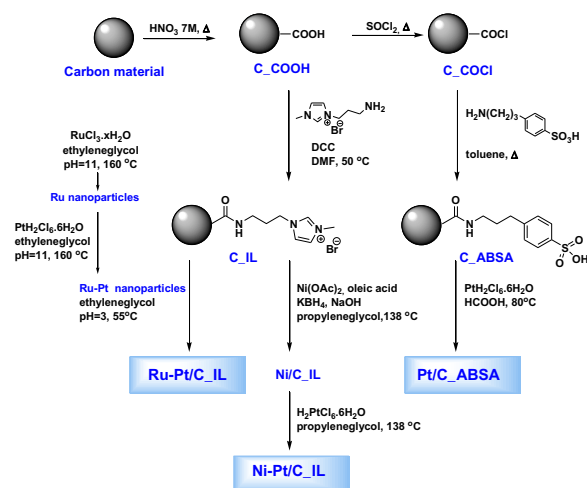


Fig. 1. Functionalization of carbon supports and synthesis procedure used for Pt, Pt-Ru and Pt-Ni catalyst used in this work.

### 3. Electrode preparation and characterization

The working electrodes were prepared using glassy carbon rods where an ink of the catalytic powders is deposited. The ink used in this work was prepared by dissolving 10 mg of the catalyst powder in 500  $\mu\text{L}$  of isopropanol plus 10  $\mu\text{L}$  of a Nafion alcoholic solution at 5 wt.%. The emulsion was sonicated for 30 minutes before the deposition of the aliquot on the electrode

surface. Finally, the electrodes were dried at 50 °C for 2 h. The electrodes were weighted before and after the power deposition to determine the catalyst weight per unit area.

The physical characterization of the catalysts was usually performed by scanning electronic microscopy (SEM), X-ray diffraction (XRD) and transmission electronic microscopy (TEM). Table 2 summarizes the techniques for catalyst characterization including electrochemical techniques.

In this work the physical characterization was performed using a JEOL 8500F FEG instrument, with associated Energy Dispersive X-Ray Spectroscopy (EDX). XRD was executed using a Rigaku Geigerflex D/MAX III C diffractometer using Cu-K $\alpha$  radiation and TEM observation were performed with a Hitachi H-8100 microscope.

For the electrochemical characterization a PAR potentiostat (model 273) controlled by a PC computer with the “Corrview” software was used. An electrochemical Greene type cell with a three-electrode configuration was used, where the auxiliary electrode was a platinum sheet and the reference was a commercial Ag/AgCl saturated electrode. The standard electrochemical characterization is carried using cyclic voltammetry, which is surface specific and is used to activate the catalysts, to determine the electrochemical active surface area and to characterize the activity and stability of the catalysts regarding the MOR and ORR. Before the determination of any electrochemical parameter, the catalysts were always activated by repeated potential cycling (30 cycles) from -0.2 to +1 V Ag/AgCl<sub>sat</sub>, at 0.050 V s<sup>-1</sup> in a 0.5 M H<sub>2</sub>SO<sub>4</sub> solution saturated with N<sub>2</sub>. The electrochemical active surface area (ECSA) of the catalysts was determined from the quotient of the desorption charge in the voltammograms to the charge of a monolayer of hydrogen atoms on the platinum nanoparticles, taken into account a reference value of 210 mC cm<sup>-2</sup>. The voltammograms were run in the same solution and experimental conditions as for the activation.

ECSA was also determined CO stripping cyclic voltammetry, which was carried out at 0.010 V s<sup>-1</sup>, from -0.2 to 1 V Ag/AgCl<sub>sat</sub> in 0.5 M H<sub>2</sub>SO<sub>4</sub>. Prior to performing these voltammograms the solution was firstly purged with CO whilst the working electrode was kept at 0.1 V Ag/AgCl<sub>sat</sub> during 40 min followed by N<sub>2</sub> purging for 10 minutes, in order to remove any CO excess from the solution. The reference charge per unit area for a monolayer of CO adsorbed on Pt, used to estimate the ECSA, was 420 mC cm<sup>-2</sup>.

The MOR was evaluated by cyclic voltammetry in a solution of 0.5 M H<sub>2</sub>SO<sub>4</sub> + 1 M CH<sub>3</sub>OH saturated with N<sub>2</sub>. The oxygen reduction reaction (ORR) was studied in a 0.5 M H<sub>2</sub>SO<sub>4</sub> solution saturated with O<sub>2</sub>; a rotating disk electrode (RDE) model 616 from PAR was used. Curves were run between + 0.8 and +0.1 V Ag/AgCl, at various disk rotating speeds, in the interval from 600 to 2400 rpm at 0.010 V s<sup>-1</sup>. All the experiments were performed at room temperature.

Table 2. Catalyst characterization techniques used in this work and obtained information.

Techniques	Obtained information
	Metal crystallite size
X-ray diffraction (XRD)	Metal lattice parameter (degree of alloying)
Scanning electron microscopy with associated to Energy Dispersive X-Ray Spectroscopy (SEM/EDX)	Aggregate morphology Elemental composition
Transmission electron microscopy (TEM)	Particle size distribution Aggregate morphology
Electrochemical	ESCA and ESCA loss CO stripping Electroactivity and stability

#### 4. Particle size effect

A number of papers have been dedicated to study the effect of Pt particle size and its influence on the specific mass activity and surface area. The effect will be herein briefly discussed taken into account 3 of the main reactions in DMFCs: ORR, MOR and COR.

For the ORR, Pt surface modification during particle size change is believed to be on the basis of the effect observed on activity and electrochemical durability of Pt/C catalysts in PEMFCs. The surface area decreases with the increase in particle size, but the mass activity for ORR has been observed to achieve a maximum when the particle size of Pt is approximately 3 nm and the specific surface area is close to 90 m<sup>2</sup>g<sup>-1</sup> [45].

This is proposed to be due to a change induced in the adsorption of OH<sub>ads</sub> (inhibitive species for ORR) [46]. On the other hand, some authors claim that there is a constant specific activity of Pt for ORR when the intercrystallite distance is greater than 20 nm [47]. In this view part of the active sites are lost when Pt catalyst particles are close together and their radial diffusion fields for O<sub>2</sub> overlap, resulting so in a decreased specific activity for ORR [47].

Also of significance is that particle size growth leads to a reduction in surface free energy. An enhancement

in the durability is demonstrated due to rapidly changing Gibbs-Thomson energies in the region from 2–3 nm to 4–5 nm particle sizes [48], which suggests gains in stability as particle size increases, worthy to take into account in designing an optimal fuel cell catalyst.

The particle size effect on the surface structure change in Pt electrocatalyst has been studied according to the model proposed by Van Hardeveld et al. [49]. The fraction of face atoms and defects on the surface were calculated as a function of particle size for cuboctahedron Pt nanoparticles. The simulation curves show that the fraction of defects decreases with the increase in Pt diameter. The adsorption of the oxygenated species on the surface is weakened by this change [50,51] and as a consequence there is an improvement of the surface specific activity of Pt.

The effect of particle size is herein exemplified with results obtained in this work with catalyst Pt/C\_ABSA of sizes 3.0 and 4.1 nm, synthesized according to procedures summarized in figure 1. Figure 2 shows cyclic voltammograms (CVs) run at  $0.050 \text{ V s}^{-1}$  in  $0.5 \text{ M H}_2\text{SO}_4$  solution saturated with  $\text{N}_2$ , for both particle size catalysts, after due activation of the electrode by potential cycling as indicated in section 3. The CVs exhibit Pt typical features, with well-defined peaks corresponding to hydrogen adsorption-desorption and Pt surface oxidation regions as well as the double layer region. The ECSA values were calculated from the charge associated to hydrogen desorption in the respective CVs. The Pt utilization factor was determined taken into account the surface area (SA) estimated using the TEM mean particle size [21]. The catalyst with larger particle size (Pt/C\_ABSA 4.1 nm) has the lower SA but a higher ECSA resulting in a Pt utilization factor of nearly 80 % against 46 % for the same catalyst with a 3.0 nm particle size, see Table 3.

Table 3. The platinum utilization factor and particle size for Pt/C\_ABSA catalyst.

Particle size /nm	SA/ $\text{m}^2\text{g}^{-1}$	ECSA/ $\text{m}^2\text{g}^{-1}$	Pt utilization factor
3.0	93.46	42.90	0.46
4.1	68.38	53.80	0.79

As a result of the mentioned increase in particle size, there is a two-fold increase in the mass activity for methanol oxidation ( $1 \text{ M CH}_3\text{OH} + 0.5 \text{ M H}_2\text{SO}_4 \text{ N}_2$  saturated solutions), as evident in figure 3.

The effect of particle size on the MOR has been attributed to the increased strength of adsorption of

both  $\text{CO}_{\text{ads}}$  and  $\text{OH}_{\text{ads}}$  on Pt with particles size lower than 5 nm [52], as well as the “ensemble effect”, where dehydrogenation is impeded by the sharp decrease of availability of contiguous Pt terrace sites for Pt particle lower than 4 nm [53].

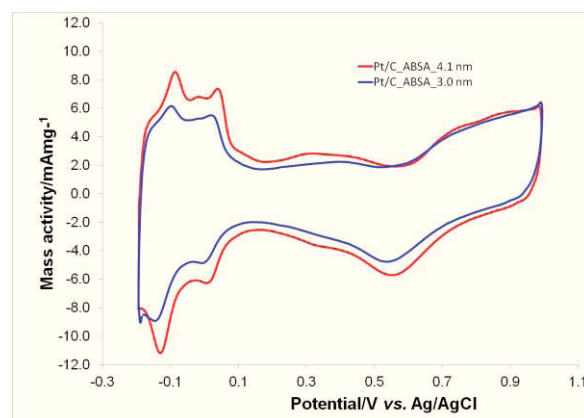


Fig. 2. Cyclic voltammograms, after catalyst activation, in a  $0.5 \text{ M H}_2\text{SO}_4$  solution for catalysts Pt/C\_ABSA of different particle size.

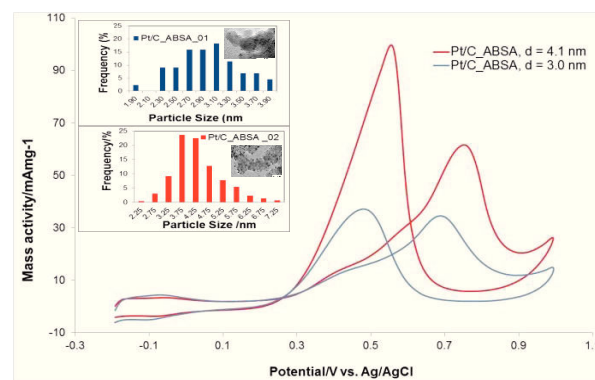


Fig. 3. Voltammetric profile for Pt/C\_ABSA catalysts in a  $0.5 \text{ M H}_2\text{SO}_4 + 1 \text{ M CH}_3\text{OH}$  solution at a scan rate of  $0.050 \text{ V s}^{-1}$ , showing the effect of particle size on methanol oxidation mass activity.

Effects on the particle size for CO oxidation has been reported for Pt nanocatalysts by a positive shift in the CO stripping peak and a decrease in MOR oxidation rate on smaller Pt particles [54,55] but contrasting views are supported in the literature regarding the role of CO energetics [55] (restricted  $\text{CO}_{\text{ads}}$  mobility as a result of stronger binding energy for CO on Pt sites) vs defect sites (ability to dissociate water and form  $\text{OH}_{\text{ads}}$ ) for particles below 2 nm.

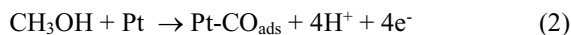
Although the significant role of defects has been noted for Pt in CO oxidation, the influence of surface diffusion rate/CO binding energy on CO oxidation kinetics cannot be ignored for those surface structures

with low CO diffusion rates [56]. Therefore, designing a new CO and methanol oxidation catalyst needs to consider the requirements of a weakly bonded state of CO<sub>ads</sub> on the Pt surface and sufficient supply of reactive hydroxyl adsorbed species at low potentials by introducing a more oxophilic atom and/or controlling the particle size and shape [57].

## 5. Improved electroactivity of Pt-based catalysts as anode materials for the MOR

### 5.1. Pt catalyst poisoning

Platinum poisoning is a consequence of adsorbed chemical species on the catalyst atoms that inhibit any posterior reactions. The oxidative removal of CO<sub>ads</sub> on the Pt surface, see reactions 2 to 4, plays a key role in determining the MOR activity, since as already stated the adsorption of CO leads to catalyst deactivation. To accomplish full oxidation and hinder poisoning it is necessary to provide hydroxyl ions to complete the reaction.



So, the binding energy of CO<sub>ads</sub> and the availability of OH<sub>ads</sub> on the catalytic surface jointly govern the kinetics of CO oxidation, which being a structure-sensitive reaction is influenced by a number of variables within which crystal face, type of surface defects and the size, shape and composition of catalyst nanoparticles [58-61].

Figure 4 shows potential shift regarding CO oxidation for own synthesized Pt catalyst, Pt/C\_ABSA.

The catalyst is active in methanol oxidation and with mass activities within the range of those obtained by Pt-Ru alloys catalysts, as evident in figure 3. Pt/C\_ABSA exhibits its capability to process CO at lower potentials than counterpart commercial catalyst with the same Pt loading.

In the next section the introduction of a second metal to form an alloy, reduce Pt loading and hinder CO poisoning will be introduced using Pt–Ru alloys since they has been identified to be one of the most effective for the MOR.

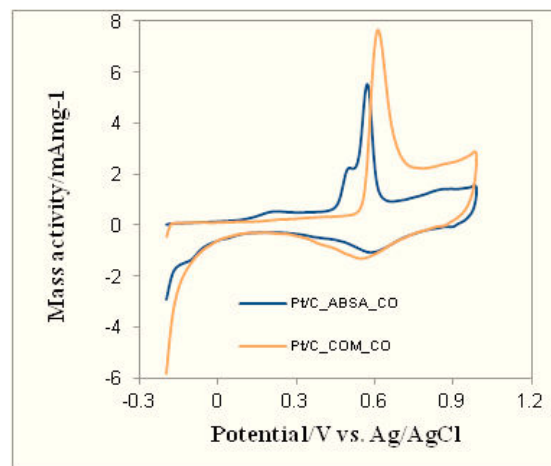
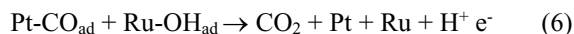


Fig. 4. CO stripping curves in 0.5 M H<sub>2</sub>SO<sub>4</sub> for catalyst Pt/C\_ABSA. Comparison is made with a commercial catalyst with the same platinum content showing potential shift for CO oxidation.

### 5.2. Pt alloying

The addition of ruthenium to the platinum in the composition of the nanoparticles has been referred as the winner combination for the MOR independently of carbon substrate [37,62-66], even though many other combinations of two or more metals have been showing better performance than Pt [63,67-71]. The advantage promoted by Ru is credited to the bifunctional mechanism and ligand effect [72-74]. The first effect is due to the higher affinity of Ru for the adsorption of oxygen atoms from hydroxyl groups which are necessary to the CO oxidation. Ru could produce active OH<sub>ads</sub> at a low potential to react with adsorbed intermediates on neighboring Pt sites:



The second effect is related to the change of platinum interatomic distance due to the incorporation of Ru atoms in the Pt crystal structure, changing the binding energies of the Pt intermediary species such as Pt-CO or Pt-OH and favoring the complete oxidation of CO. So, tolerance to CO poisoning is promoted by the alloying of the two metals since part of the improving effect is directly related to the interatomic distance and strain between the Ru and Pt atoms [75,76]. This electronic effect could enhance methanol dehydrogenation on Pt sites and weaken the adsorption strength of CO<sub>ads</sub>. Another concern is the oxidation state of Ru. Some studies have emphasized the role of the metallic state of Ru, in others hydrous ruthenium oxide (RuO<sub>x</sub>H<sub>y</sub>) plays a more important role than metallic Ru in the bifunctional mechanism [59].

One way of promoting the alloying is through a heat treatment under a reducing atmosphere [77-80]. The heating also promotes the growth of the metal nanoparticles with a consequent decrease of active surface area, so both features have to be optimized to achieve the best effect for methanol oxidation. Figure 5 depicts the outcome obtained on a catalyst Ru-Pt/C (10:20) before and after thermal treatment at 400°C. The improvement on methanol oxidation is visible on the increase on the peak current density of the voltammogram obtained in acid media and the TEM micrographs show the corresponding increase of the particle size. The peak potential is shifted to the anodic side of the voltammogram which reflects a possible increase on platinum content on the nanoparticles surface area similar to the effect found in core-shell nanoparticles structure [81-85].

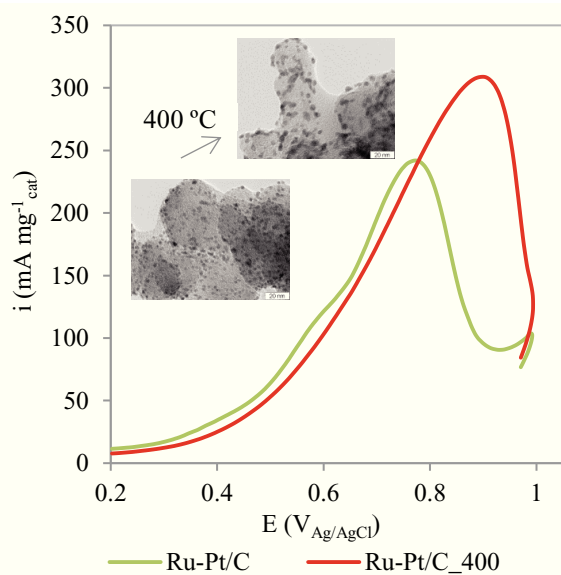


Fig. 5. Voltammograms showing the increase of the peak current on methanol oxidation in acid media due to catalyst heat treatment at 400°C. Insets show the TEM micrographs where the corresponding increase of particle size is visible.

The use of carbon nanotubes introduces a larger surface area for CO oxidation. In this work, equivalent treatment was given to MWCNTs to that applied to Ru-Pt/C. Better results were obtained for MWCNTs regarding not only the surface area for CO oxidation but also the alloying degree and consequently higher mass activity for MOR. Furthermore, only an 11% is reported for the activity loss after 4000 cycles in methanol acidic solutions which indicates superior stability of MWCNTs supported Ru-Pt catalyst for MOR than for the counterpart supported on Vulcan [86].

## 6. Enhanced electroactivity of Pt-based catalysts as cathode materials for the ORR

### 6.1. Mechanisms

The necessary reaction to close the electrochemical circuit in the DMFCs is the oxygen reduction at the cathode, which in acid media occurs according to the following reaction:



So far, platinum is among the best catalysts even though the reaction is still sluggish [14, 87-90]. Different mechanisms involving complex intermediary steps can occur [90], see figure 6, but the dissociative mechanism can be considered the more efficient. This mechanism involves four electrons and releases two water molecules, according to the following reactions:



The associative mechanism, where  $\text{H}_2\text{O}_2$  is formed as an intermediary product, is described by the following reactions:



In this mechanism, reaction 12 is necessary to complete the reduction of oxygen to water, whereas reaction 13 corresponds to a disproportionation reaction with no electrons involved.

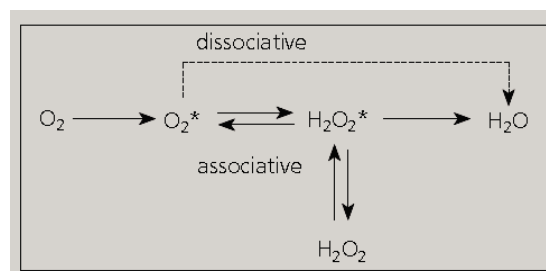


Fig. 6. Schematics of ORR dissociative and associative mechanisms.

The electrochemical characterization of the ORR is usually performed through the use of the rotating disk electrode (RDE). The reaction follows the Koutecky-Levich theory [91] with the diffusion current density expressed by the following equation:

$$\frac{1}{i_d} = \frac{1}{0.62 n F v^{-1/6} D_{O_2}^{2/3} C_{O_2} \omega^{1/2}} \quad (14)$$

where  $i_d$  is the diffusion current density,  $n$  the number of electrons exchanged per mole of  $O_2$ ,  $F$  the Faraday constant,  $v$  the kinematic viscosity of the electrolyte,  $D_{O_2}$  the oxygen diffusion,  $C_{O_2}$  the bulk oxygen concentration in the electrolyte and  $\omega$  the rotation speed of the electrode. Different curves are obtained by varying the electrode rotation speed and from the slope of experimental plot of  $1/i_d$  vs.  $1/\omega^{1/2}$  the number of exchange electrons can be estimated. Figure 7 shows the data obtained for the commercial catalyst Pt/C 10 wt.% where the estimated number of electrons found was 4.

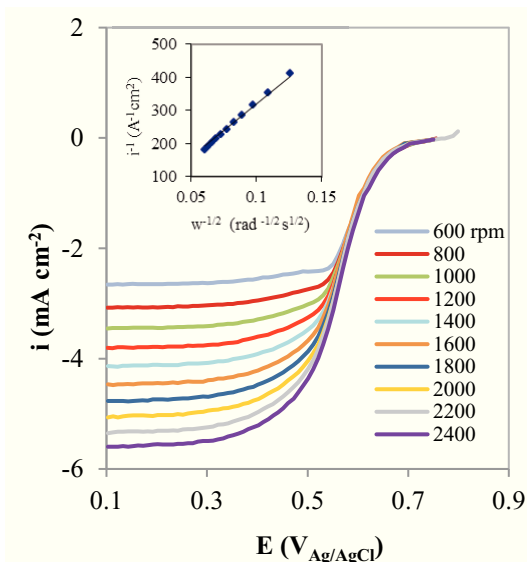


Fig. 7. RDE voltammetry for the ORR obtained at  $0.010 \text{ Vs}^{-1}$  in  $0.5 \text{ M H}_2\text{SO}_4$  ( $O_2$  saturated) at various rotating speeds (b). Inset shows plot  $i_d^{-1}$  vs  $\omega^{-1/2}$  in agreement with the Levich equation.

### 6.2. Pt alloying

Searching for alternatives to pure platinum catalysts for the ORR for enhanced performance at lower cost continues to be a goal. Even though core-shell Ru-Pt/C catalysts have been reported as possible cathode catalysts [90,92,93], other metal pairs have revealed good activity for ORR such as the Pt-Ni, Pt-Co or Pt-Cr combinations [33,91,94-96]. The causes that promote the beneficial effect are multiple and include the size and the structure of the nanoparticle, the alloying degree and changes in the strain of the Pt-Pt bond [84]. Figure 8 shows the voltammograms obtained for the oxygen reduction obtained in RDE at 2400 rpm for the catalysts Pt/C (10 wt.%) and

Ni@Pt/C (10:10) where it is visible the increase in the diffusion current density promoted by platinum nickel alloying.

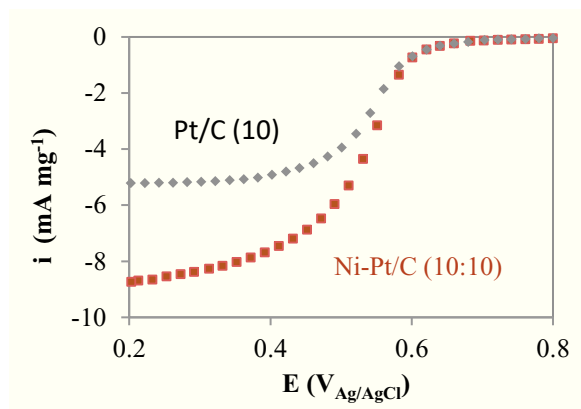


Fig. 8. Linear polarization curves for NiPt/C 10:10 wt.% and Pt/C 10 wt.% catalyst, RDE (2400 rpm).

## 7. Final Comments

Catalysts technology at the present state is considered insufficient to support large-scale production of efficient DMFCs.

This paper presents a brief account of some of the most effective routes for improving the performance of catalysts for DMFCs including catalyst support diversification and functionalization, control of particle size and the introduction of Pt alloying and heat treatment, in order to enhance the rate of critical reactions such as CO electrooxidation and the oxygen reduction reaction and also to reduce Pt loading.

Despite the large number of published works and promising advances obtained, it is still necessary to overcome constraints regarding cost, efficiency and life-time durability of catalysts for use in DMFCs by better understanding the relationship between composition/structure and electroactivity. In-depth studies on durability and identification of the main catalysts/electrodes degradation mechanism are still required for the furthering of effective mitigating strategies that might contribute to foster practical applications.

## Acknowledgements

The present work is financed by FEDER funds through Programa Operacional Factores de Competitividade-COMPETE and by National Funds through Fundação para a Ciência e Tecnologia (FCT) Project PTDC/CTM-ENE/1585/2012.

## References

- [1] A. Goepfert, M. Czaun, J.P. Jones, G.K.S. Prakash, G.A. Olah, *Chem. Sov. Rev.* 43 (2014) 8084.
- [2] W. Wang, S. Wang, X. Ma, J. Gong, *Chem. Soc. Rev.* 40 (2011) 3703.
- [3] J. Kim, C.A. Henao, T.A. Johnson, D.E. Dedrick, J.E. Miller, E.B. Stecheld, C.T. Maravelias, *Energy Environ. Sci.* 4 (2011) 3122.
- [4] A.S. Aricò, V. Baglio, V. Antonucci, in: *Electrocatalysis of Direct Methanol Fuel Cells*. H. Liu and J. Zhang editors, Wiley-VCH Verlag GmbH & Co., Weinheim, 2009.
- [5] H.R. Corti, E.R. Gonzalez in: *Direct Alcohol Fuel Cells: Materials, Performance, Durability and Applications*, H.R. Corti and E.R. Gonzalez Editors, Springer, New York, London, 2014.
- [6] S.M. Karamundi, F. Achmad, W.R.W. Daud, *Int. J. Hydrogen Energy* 34 (2009) 6902.
- [7] C.K. Dyer, *J. Power Sources* 136 (2004) 386.
- [8] P. Kumar, K. Dutta, S. Das, P.P. Kundu, *Int. J. Energy Res.* (2014) DOI: 10.1002/er.3163.
- [9] [http://www.researchandmarkets.com/research/vvx/hcg/direct\\_methanol](http://www.researchandmarkets.com/research/vvx/hcg/direct_methanol), accessed July 2016.
- [10] S. Srinivasan, *Fuel cells: From Fundamentals to Applications*, Springer, USA, 2006.
- [11] H.S. Liu, J.J. Zhang, *Electrocatalysis of Direct Methanol Fuel Cells: From Fundamentals to Applications*, Wiley-VCH, Germany, 2009.
- [12] R.N. Singh, R. Awasthi, C.S. Sharma, *Int. J. Electrochem. Sci.* 9 (2014) 5607.
- [13] N. Kakati, J. Maiti, S.H. Lee, S.H. Jee, B. Viswanathan, Y.S. Yoon, *Chem. Rev.* 114 (2014) 12397.
- [14] N. Ramaswamy, S. Mukerjee, *Advances in Physical Chemistry* (2012), Article ID 491604, 17 pages.
- [15] Y. Nie, L. Li, Z. Wei, *Chem. Soc. Rev.* 44 (2015) 2168.
- [16] D.C. Higgins, Z. Chen, *Can. J. Eng. Chem.* 91 (2013) 1881.
- [17] H. Huang, X. Wang, *J. Mater. Chem. A* 2 (2014) 6266.
- [18] S. Zhang, Y. Shao, G. Yin, Y. Lin, *J. Mater. Chem. A* 1 (2013) 4631.
- [19] S. Sharma, B.G. Pollet, *J. Power Sources* 208 (2012) 96.
- [20] M.S. Saha, V. Neburchilov, D. Ghosh, J. Zhang, *WIREs Energy Environ.* 2 (2013) 31.
- [21] A. Capelo, M.A. Esteves, A.I. de Sá, R.A. Silva, L. Canguero, A. Almeida, R. Vilar, C.M. Rangel, *Int. J. Hydrogen Energy* 41 (2016) 12962.
- [22] N.W.S. Kam, T.C. Jessop, P.A. Wender, H. Dai, *J. Am. Chem. Soc.* 126 (2004) 6850.
- [23] J.D. Lu, M.C. Yang, *J. Power Sources* 196 (2011) 7450.
- [24] M.S. Saha, A. Kundu, *J. Power Sources* 195 (2010) 6255.
- [25] Z. Yang, H. Nie, X. Chen, X.H. Chen, S. Huang, *J. Power Sources* 236 (2013) 238.
- [26] X. Wang, B. He, Z. Hu, Z. Zeng, S. Han, *Sci. Technol. Adv. Mater.* 15 (2014) 043502.
- [27] A.G. Gonçalves, J.L. Figueiredo, J.J.M. Órfão, M.F.R. Pereira, *Carbon* 48 (2010) 4369.
- [28] J.C. Calderón, G. García, L. Calvillo, J.L. Rodríguez, M.J. Lázaro, E. Pastor, *App. Catal., B: Environmental* 165 (2015) 676.
- [29] C. Alegre, M.E. Gálvez, R. Moliner, M.J. Lázaro, *Catalysts* 5 (2015) 392.
- [30] M. Harada, H. Einaga, *J. Colloid Interf. Sci.* 308 (2007) 568.
- [31] D. Nagao, Y. Shimazaki, S. Saeki, Y. Kobayashi, M. Konno, *Colloid Surf. A* 302 (2007) 623.
- [32] Y. Chen, Z. Liang, F. Yang, Y. Liu, S. Chen, *J. Phys. Chem. C* 115 (2011) 24073.
- [33] D. Sébastien, M.J. Lázaro, R. Moliner, I. Suelves, A.S. Aricò, V. Baglio, *Int. J. Hydrogen Energy* 39 (2014) 5414.
- [34] W.H. Lizcano-Valbuena, V.A. Paganin, E.R. Gonzalez, *Electrochim. Acta* 47 (2002) 3715.
- [35] L. Santos, F. Colmati, E.R. Gonzalez, *J. Power Sources* 159 (2006) 869.
- [36] J.C. Calderón, N. Mahata, M.F.R. Pereira, J.L. Figueiredo, V.R. Fernandes, C.M. Rangel, L. Calvillo, M.J. Lázaro, E. Pastor, *Int. J. Hydrogen Energy*, 37 (2012) 7200.
- [37] X. Wang, I.M. Hsing, *Electrochim. Acta* 47 (2002) 2981.
- [38] C. Li, Z. Shao, M. Pang, C. T. Williams, X. Zhang, C. Liang, *Ind. Eng. Chem. Res.* 51 (2012) 4934.
- [39] S. Yan, G. Sun, J. Tian, L. Jiang, J. Qi, Q. Xin, *Electrochim. Acta* 52 (2006) 1692.
- [40] Z. Liu, L. Hong, *J. Appl. Electrochem.* 37 (2007) 505.
- [41] H. Li, G. Sun, L. Cao, L. Jiang, Q. Xin, *Electrochim. Acta* 52 (2007) 6622.
- [42] P. Kanninen, M. Borghei, V. Ruiz, E.I. Kauppinen, T. Kallio, J. Yi, *Int. J. Hydrogen Energy* 37 (2012) 19082.
- [43] L. Demarconnay, C. Coutanceau, J.M. Léger, *Electrochim. Acta* 53 (2008) 3232.
- [44] S.M. Senthil Kumar, J. Soler Herrero, S. Irusta, K. Scott, *J. Electroanal. Chem.* 647 (2010) 211.
- [45] K. Kinoshita, *J. Electrochem. Soc.* 137 (1990) 845.
- [46] H.A. Gasteiger, S.S. Kocha, B. Sompalli and F.T. Wagner, *Appl. Catal. B* 56 (2005) 9.
- [47] H. Yano, T. Akiyama, H. Uchida and M. Watanabe, *Energy Environ. Sci.* 3 (2010) 1511.
- [48] E.F. Holby, W. Sheng, Y. Shao-Horn and D. Morgan, *Energy Environ. Sci.* 2 (2009) 865.
- [49] R. Van Hardeveld, F. Hartog, *Surf. Sci.* 5 (1969) 189.
- [50] J.K. Norskov, J. Rossmeisl, A. Logadottir, L. Lindqvist, J.R. Kitchin, T. Bligaard, H. Jonsson, *J. Phys. Chem. B* 108 (2004) 17886.
- [51] V.R. Stamenkovic, B. Fowler, B.S. Mun, G.F. Wang, P.N. Ross, C.A. Lucas, N.M. Markovic, *Science* 315 (2007) 493.
- [52] S. Mukerjee and J. McBreen, *J. Electroanal. Chem.* 448 (1998) 163.

- [53] S. Park, Y. Xie and M. J. Weaver, *Langmuir* 18 (2002) 5792.
- [54] M. Arenz, K.J.J. Mayrhofer, V. Stamenkovic, B.B. Blizanac, T. Tomoyuki, Ph.N. Ross and N.M. Markovic, *J. Am. Chem. Soc.* 127 (2005) 6819.
- [55] F. Maillard, M. Eikerling, O.V. Cherstiouk, S. Schreier, E. Savinova and U. Stimming, *Faraday Discuss.* 125 (2004) 357.
- [56] S.C.S. Lai, N.P. Lebedeva, T.H.M. Housmans and M. T. M. Koper, *Top. Catal.* 46 (2007) 320.
- [57] N.M. Markovic and P.N. Ross, *Surf. Sci. Rep.* 45 (2002) 117.
- [58] J. Solla-Gullon, F.J. Vidal-Iglesias, A. Lopez-Cudero, E. Garnier, J.M. Feliu and A. Aldaza, *Phys. Chem. Chem. Phys.* 10 (2008) 3689.
- [59] X. Zhao, M. Yin, L. Ma, L. Liang, Ch. Liu, J. Liao, T.G. Luc and W. Xing, *Energy Environ. Sci.* 4 (2011) 2736.
- [60] J. R. Anderson, M. Boudart in: *Catalysis: Science and Technology*, Springer Verlag, Berlin, New York (1982).
- [61] C.A. Lucas, N.M. Markovic, P.N.R. Ross, *Surface Science* 425 (1999) L381.
- [62] J.N. Tiwari, R.N. Tiwari, G. Singh, K.S. Kim, *Nano Energy* 2 (2013) 2.
- [63] O.A. Petri, *J. Solid State Electrochem.* 12 (2008) 609.
- [64] M.M. Tusi, N.S.O. Polanco, M. Brandalise, O.V. Correa, J.C. Villalba, F.J. Anaissi, A.O. Neto, E.V. Spinace, *Int. J. Electrochem. Sci.* 6 (2011) 484.
- [65] X. Xue, T. Lu, C. Liu, W. Xu, Y. Su, Y. Lv, W. Xing, *Electrochim. Acta* 50 (2005) 3470.
- [66] L. Meng, D. Cao, W. Liu, Y. Zhang, M. Zhao, *Ionics* 20 (2014) 1127.
- [67] A.O. Neto, R.R. Dias, M.M. Tusi, M. Linardi, E. V. Spinac, *J. Power Sources* 166 (2007) 87.
- [68] M. Zhu, G. Sun, Q. Xin, *Electrochim. Acta* 54 (2009) 1511.
- [69] J. Kang, R. Wang, H. Wang, S. Liao, J. Key, V. Linkov, S. Ji, *Materials* 6 (2013) 2689.
- [70] Z. Yin, Y. Zhang, K. Chen, J. Li, W. Li, P. Tang, H. Zhao, Q. Zhu, X. Bao, D. Ma, *Scientific Reports*, 4 Article number: 4288 (2014) doi: 10.1038/srep04288.
- [71] Y. Liang, H. Zhang, H. Zhong, X. Zhu, Z. Tian, D. Xu, B. Yi, *J. Catalysis* 238 (2006) 468.
- [72] C. Roth, A.J. Papworth, I. Hussain, R.J. Nichols, D.J. Schiffrin, *J. Electroanal. Chem.* 581 (2005) 79.
- [73] F.J. Scott, S. Mukerjee, D.E. Ramaker, *J. Phys. Chem. C* 114 (2010) 442.
- [74] C. Roth, N. Benker, R. Theissmann, R.J. Nichols, D. J. Schiffrin, *Langmuir* 24 (2008) 2191.
- [75] C.T. Hsieh, Y.S. Chang, K.M. Yin, *J. Phys. Chem. C* 117 (2013) 15478.
- [76] R.G. Freitas, E.P. Antunes, E.C. Pereira, *Electrochim. Acta* 54 (2009) 1999.
- [77] Y.C. Wei, C.W. Liu, K.W. Wang, *ChemPhys Chem* 10 (2009) 1230.
- [78] M.K. Jeon, K.R. Lee, H.J. Jeon, S.I. Woo, *J. Appl. Electrochem.* 39 (2009) 1503.
- [79] M. Tsypkin, J.L.G. de la Fuente, S.G. Rodríguez, Y. Yu, P. Ochal, F. Seland, O. Safonova, N. Muthuswamy, M. Rønning, D. Chen, S. Sunde, *J. Electroanal. Chem.* 704 (2013) 57.
- [80] E. Antollini, F. Cardellini, *J. Alloys Comp.* 315 (2001) 118.
- [81] T.Y. Chen, T.L. Lin, T.J.M. Luo, Y. Choi, J.F. Lee, *ChemPhysChem* 11 (2010) 2383.
- [82] P. Ochal, J.L.G. de la Fuente, M. Tsypkin, F. Seland, S. Sunde, N. Muthuswamy, M. Rønning, D. Chen, S. Garcia, S. Alayoglu, B. Eichhorn, *J. Electroanal. Chem.* 655 (2011) 140.
- [83] N. Muthuswamy, J.L.G. Fuente, D.T. Tran, J. Walmsley, M. Tsypkin, S. Raen, S. Sunde, M. Rønning, D. Chen, *Int. J. Hydrogen Energy* 38 (2013) 16631.
- [84] D. Bokach, J.L.G. de la Fuente, M. Tsypkin, P. Ochal, I.C. Endsjø, R. Tunold, S. Sunde, F. Seland, *Fuel Cells* 11 (2011) 735.
- [85] S. Goto, S. Hosoi, R. Arai, S. Tanaka, M. Umeda, M. Yoshimoto, Y. Kudo, *J. Phys. Chem. C* 118 (2014) 2634.
- [86] M.A. Esteves, A.I. de Sá, A. Capelo, L. Canguero, A. Almeida, R. Vilar, M.J. Lázaro and C.M. Rangel, (submitted) 2016.
- [87] M. Shao, Q. Chang, J.P. Dodelet, R. Chenitz, *Chem. Rev.* 116 (2016) 3594.
- [88] Y. Holade, N.E. Sahin, K. Servat, T.W. Napporn, K.B. Kokoh, *Catalysts* 5 (2015) 310.
- [89] A.M. Gómez-Marín, R.Rizo, J.M. Feliu, *Beilstein J. Nanotechnol.* 4 (2013) 956.
- [90] W. Xing, G. Ying, J. Zhang, *Rotating Electrode Methods and Oxygen Reduction Electrocatalysts*, Elsevier Science, Amsterdam, 2014.
- [91] J. Zhang (Ed.), *Fuel Cell Electrocatalyst and Catalyst Layers*, Springer, London, 2008.
- [92] P. Strasser, S.Kuhl, *Nano Energy* 29 (2016) 168-177
- [93] K. A. Kuttiyiel, Y. Choi, K. Sasaki, D. Su, S. Hwang, S. Yim, T. Yang, G. Park, Ra. R. Adzic, *Nano Energy* 29 (2016) 261-267
- [94] L. Yang, M.B. Vukmirovic, D. Su, K. Sasaki, J.A. Herron, M. Mavrikakis, S. Liao, R.R. Adzic, *J. Phys. Chem.* 117 (2013) 1748.
- [95] D. Wang, H.L. Xin, R. Hovden, H. Wang, Y. Yu, D.A. Muller, F.J. Di Salvo, H.D. Abruna, *Nature Materials* 12 (2013) 81.
- [96] H. Lv, D. Li, D. Strmcnik, A.P. Paulikas, N.M. Markovic, V.R. Stamenkovic, *Nano Energy* 29 (2016) 149.